Journal of Physiology (1988), **407**, *pp.* 405–432
With 12 *text-figures*
Printed in Great Britain

TWO-SUCTION-ELECTRODE VOLTAGE-CLAMP ANALYSIS OF THE SUSTAINED CALCIUM CURRENT IN CAT SENSORY NEURONES

BY W. ROWLAND TAYLOR*

From the Department of Physiology, John Curtin School of Medical Research, Australian National University, Canberra, A.C.T. 2601, Australia

(*Received 19 January 1988*)

SUMMARY

1. The kinetics of the sustained calcium current were examined in cat dorsal root ganglion (DRG) neurones, using a two-suction-electrode voltage clamp. It was shown that this current could be examined with minimal contamination from other ionic currents. Experiments were performed at 20 °C, with a concentration of 10 mM-calcium externally.

2. The transient calcium current was eliminated by using a holding potential of −50 mV. The sustained calcium current showed no evidence of steady-state inactivation at potentials between −90 and −30 mV.

3. The activation and deactivation time course of the calcium current was described by a double-exponential function. The activation process was examined without interference from significant inactivation under the conditions used.

4. The steady-state activation of the calcium channels was approximated by a two-step activation process. Both reactions were voltage sensitive, the first having an equivalent valency of $3{\cdot}4 \pm 0{\cdot}1$ electronic charges (e^-), and the second with an equivalent valency of $1{\cdot}0 \pm 0{\cdot}2$ e^-. On average, half-maximal channel activation occurred at +10 mV.

5. The fast and the slow time constants of the exponential relaxations differed by a factor of 4–10 and both showed significant voltage dependence. Both the fast and slow time constants were greatest at potentials where approximately half the available channels were activated in the steady state. The slow time constant measured from activation and deactivation appeared to be independent of the starting potential.

6. The fractional amplitude of the slow exponential component of the tail currents was $0{\cdot}09 \pm 0{\cdot}01$ at −70 mV and increased steadily at more positive potentials passing through a clear maximum of $0{\cdot}59 \pm 0{\cdot}03$ at −10 mV.

7. Reducing the temperature decreased the magnitude of the peak inward current, with an apparent activation energy (E_a) of 67 kJ/mol. The slow time constants measured from activation and deactivation were also reduced at lower temperatures. The slow activation time constant had a higher temperature sensitivity (E_a = 85 kJ/mol) than the slow tail current time constant (E_a = 29 kJ/mol). The fast tail current time constant was reduced at lower temperatures with an apparent E_a of 79 kJ/mol.

* Present address: Department of Neurobiology D239, Sherman Fairchild Science Building, Stanford, CA 94305, U.S.A.

8. Application of 10 μM-(±)Bay K 8644 prolonged the tail currents and shortened the activation time constant. The calcium current was activated at more negative potentials and the slope of the steady-state activation curve was reduced.

9. Two sequential rate theory models were fitted to the data, one having two closed states preceding an open state (three-state model), and the second having three closed states preceding an open state (four-state model). The three-state model did not describe the steady-state and kinetic data accurately, while the four-state model provided an adequate description of the data.

10. The four-state model predicted a mean open time for the calcium channel of 0·5 ms at 0 mV, which depended on the membrane potential with an equivalent dipole moment of 0·56 e^-. It also predicted the presence of a short-lived intermediate closed state with a mean lifetime of 40 μs at 0 mV. The model predicted that the equivalent of 5·65 e^- move from the inside to the outside of the membrane during channel activation. The predicted gating charges were unevenly distributed across the three reaction steps.

INTRODUCTION

There have been a number of studies of the calcium current using conventional two-intracellular-microelectrode voltage clamp (Geduldig & Greuner, 1970; Standen, 1974; Kostyuk, Krishtal & Doroshenko, 1974; Adams & Gage, 1979; Connor, 1979). These pioneering studies relied on external pharmacological agents to suppress the other ionic currents. Consequently they were limited by contamination of the current records, mainly by incompletely suppressed potassium currents. The development of internal perfusion techniques (Krishtal & Pidoplichko, 1976; Lee, Akaike & Brown, 1978; Hamill, Marty, Neher, Sakmann & Sigworth, 1981) largely solved this problem with the added advantage that the time resolution of the voltage-clamp systems was improved. Descriptions of the kinetics of the sustained (slowly inactivating) calcium current in new-born rat DRG neurones (Kostyuk, Veselovsky & Tsyndrenko, 1981), clonal pituitary tumour cells (Hagiwara & Ohmori, 1982), bovine chromaffin cells (Fenwick, Marty & Neher, 1982), molluscan neurones (Brown, Tsuda & Wilson, 1983; Byerly, Chase & Stimers, 1984) and hippocampal neurones (Kay & Wong, 1987) were produced using these techniques.

There now appear to be at least three different types of calcium currents: the well-known sustained calcium current and two more recently discovered transient calcium currents (Carbone & Lux, 1984; Nowycky, Fox & Tsien, 1985; Fox, Nowycky & Tsien, 1987). Both the sustained and at least one of the transient calcium currents are present in mammalian sensory neurones (Bossu, Feltz & Thomann, 1985; Fedulova, Kostyuk & Veselovsky, 1985; Robertson & Taylor, 1986), and in this work 'calcium current' will refer to the sustained calcium current.

Aside from the studies by Kostyuk *et al.* (1981) and Kay & Wong (1987), there are very few detailed data available on the kinetic characteristics of calcium channels in freshly isolated mammalian neurones. Both these studies described the calcium current kinetics using Hodgkin–Huxley m^2 kinetics (Hodgkin & Huxley, 1952), an approach which is not considered here due to the large ratio of the activation-to-deactivation time constants observed. This study addresses the basic question: what is the minimal kinetic scheme that will account for calcium channel activity in

mammalian sensory neurones? This question has not been resolved for the calcium channel in any preparation. Previous workers have concentrated on sequential models and this approach will be used here. It has been suggested that the kinetics of the calcium channel are not consistent with three-state sequential activation schemes and a number of authors have proposed four-state schemes (Hagiwara & Ohmori, 1983; Brown *et al.* 1983; Byerly *et al.* 1984; Brown, Lux & Wilson, 1984). It was found, in agreement with earlier findings on the calcium channel in other preparations, that the kinetics of the calcium current in cat DRG neurones are not consistent with a three-state model. A specific four-state model is presented which describes the kinetic and steady-state data quantitatively. Some preliminary results have been published previously (Taylor, 1985).

METHODS

Preparation

Dorsal root ganglia (L6, L7 and S1) were removed from adult cats (1·2–2·5 kg) anaesthetized with sodium pentobarbitone. Trypsin (0·5% type IX, Sigma) and collagenase (0·5% type I A, Sigma) were dissolved in standard solution and applied to the ganglia at 30 °C for 1 h. Enzyme treatment was essential for dispersal of the cell bodies and for obtaining high sealing resistances between the suction electrodes and the cell membrane. Cells with diameters of 50–100 μm were used; there were no obvious differences in the characteristics of the calcium currents from cell to cell. After application of the two suction electrodes, cells with an input resistance greater than 5 MΩ and a resting potential more negative than −40 mV were considered acceptable for further analysis. Two minutes equilibration time was allowed before recording.

Electrodes

Suction electrodes were fabricated from 1·5 mm borosilicate haematocrit tubing. Each electrode was fire-polished on a microforge, to an internal diameter of 10–15 μm. When filled with internal solution, electrode resistance was 0·5–0·8 MΩ. Bath ground and bath voltage electrodes were simply lengths of 1 mm electrode glass filled with 3 M-KCl/agar. All electrodes were connected to electronics via Ag/AgCl pellets.

Solutions

All concentrations are given in millimolar. The pH of all solutions was 7·4.

Standard external solution: 140 NaCl; 2 KCl, 5 $CaCl_2$; 10 *N*-2-hydroxyethylpiperazine-*N*-2-ethanesulphonic acid (HEPES); 10 glucose. Calcium currents: 115 choline chloride; 25 tetraethylammonium bromide (TEA); 2 CsCl; 1 $MgCl_2$; 10 $CaCl_2$; 10 HEPES; and 10 glucose.

Internal solution: 140 CsCl; 10 TEA; 5 ethyleneglycol-bis-(β-aminoethylether)-*N*,*N*-tetraacetic acid (EGTA); and 5 HEPES.

The bath temperature was maintained at 20 °C by a peltier element. Solutions were perfused at rates of 2–3 ml/min, except when recording.

(±)Bay K 8644 (a gift from Bayer) was dissolved in ethanol to a concentration of 10 mM and quantities of this stock added directly to the external solution. An equal amount of ethanol was added to the control solution.

Voltage clamp

The voltage-clamp circuit was of conventional design, implemented using LF356 operational amplifiers. Special care was taken to minimize the input capacitance of the voltage recording end, by mounting the headstage on the micromanipulator close to the preparation, and by leaving less than 200 μm of the electrode under the bath solution. These precautions maintained a high frequency response without the need for capacitance neutralization. Capacitive coupling between the electrodes was reduced by placing a grounded aluminium shield on the current-passing electrode. Phase compensation was implemented as described by Finkel (1985), to enable higher

open-loop gain to be employed while maintaining the stability of the clamp. The open-loop gain of 400–600-fold was adequate to obtain high DC fidelity and a very rapid step response.

Typically the recorded voltage rose in 6 μs, but oscillated for about 25 μs. The rapid settling time indicated that the potential across the membrane was isopotential 25 μs after the voltage step. Membrane potential was measured differentially, between the voltage electrode and a bath voltage electrode close to the preparation, a technique which obviated any series-resistance errors introduced by the finite resistance of the bath ground electrode. The membrane current was measured using an opamp configured for current-to-voltage conversion with a 1 MΩ feed-back resistor. Although the series resistance was not measured, indirect evidence that series resistance errors were not large is shown in Fig. 2*B* of the subsequent paper, where the instantaneous current–voltage relation was independent of the size of the tail currents. Brown *et al.* (1983) estimated that the series resistance in *Helix* neurones was less than 5 kΩ. A similar value would result in tolerable voltage errors of $< 4\%$ for the largest tail currents observed here.

Excellent space clamp of the calcium current was obtained since the cells generally had less than 100 μm of axon attached. Further, although 'break-through spikes' were often encountered when sodium currents were recorded, they were never encountered when recording calcium currents. This indicated that the density of calcium channels in the axon was low, in agreement with previous work (Meves & Vogel, 1973; Junge & Miller, 1977; Dichter & Fischbach, 1977).

Data acquisition

Linear leakage and capacitive currents were subtracted by adding equal and opposite voltage pulses. In later experiments a series of small hyperpolarizing pulses ($\leqslant 30$ mV) were added together on-line until the sum of the pulses equalled the depolarizing test pulse. The current and voltage signals were filtered through a 4-pole Bessel filter at 8 kHz.

Theoretical curves were fitted to the data using a modified Levenberg–Morrison–Marquandt (LMM) algorithm (Osborne, 1976). When fitting the activation of the calcium current a digital filter was often used to further reduce the noise levels. The filter was passed forwards and backwards over the data which resulted in zero added phase shift.

Rate theory models

The two sequential models examined in this paper were based on standard Eyring rate theory (Glasstone, Laidler & Eyring, 1949). The transition rate constants were assumed to depend exponentially on the membrane potential (Stevens, 1978). The three-state model is illustrated by eqn (3) below. The four-state model simply includes an additional closed state preceding the open state. For both models the forward rate constants have odd subscripts and the backward rate constants even subscripts. Each reaction step in the kinetic schemes has two rate constants associated with it, which are related to the free-energy change by

$$k_{i,j} = \nu \exp(-\Delta G^*_{i,j}), \tag{1}$$

where $\nu = kT/h$, and

$$\Delta G^*_{i,j} = w^*_{ij} - w_{i,j} \pm z_{ij}\delta_{i,j}V_m F/RT, \tag{2}$$

where w^*_{ij} is the energy of the transition state, $w_{i,j}$ are the energy levels of the two conformations, z_{ij} is the total dipole moment of the reaction step normal to the membrane electric field and $\delta_{i,j}$ are the fractions of z_{ij} attributed to k_i and k_j respectively. The dipole moments are expressed as the equivalent electronic charge that must move across the entire membrane electric field. V_m is the electric field across the membrane, T is temperature and k, h, F and R are the usual thermodynamic constants.

The systems of linear differential equations describing the two models were solved using matrix notation, in order to obtain equations relating the observed relaxation rate constants to the model rate constants. The three-state model can be represented by the kinetic equation

$$C_1 \underset{k_2}{\overset{k_1}{\rightleftharpoons}} C_2 \underset{k_4}{\overset{k_3}{\rightleftharpoons}} O, \tag{3}$$

which shows two closed conformations (C_1 and C_2) followed by an open state (O). The system of differential equations describing eqn (3) can be written

$$f'(t) = A_{33} f(t), \tag{4}$$

where A_{33} is the coefficient matrix

$$A_{33} = \begin{bmatrix} -k_1 & k_2 & 0 \\ k_1 & -(k_2+k_3) & k_4 \\ 0 & k_3 & -k_4 \end{bmatrix},$$

$f(t)$ is a column vector with elements $C_1(t)$, $C_2(t)$ and $O(t)$ and $f'(t)$ is the first derivative of $f(t)$. The solution matrix must satisfy eqn (4) and has the form

$$\phi_{33}(t) = u_i \exp(\lambda_i t), \tag{5}$$

where u_i and λ_i are the eigenvectors and eigenvalues of A_{33} respectively.

The eigenvalues of the coefficient matrix predict the observed relaxation rate constants from the model rate constants and are obtained from the solutions to the characteristic polynomials. For the three-state model the characteristic polynomial is,

$$\lambda(\lambda^2 + (k_1+k_2+k_3+k_4)\lambda + (k_1k_3 + k_1k_4 + k_2k_4)) = 0,$$

and for the four-state model the characteristic polynomial is

$$\lambda(\lambda^3 + b\lambda^2 + c\lambda + d) = 0,$$

where $b = (k_1+k_2+k_3+k_4+k_5+k_6)$, $c = k_1(k_3+k_4+k_5+k_6) + k_2(k_4+k_5+k_6) + k_3(k_5+k_6) + k_4k_6$ and $d = k_1k_3(k_5+k_6) + k_4k_6(k_1+k_2)$.

In each case one of the eigenvalues is zero, corresponding to the time-invariant (steady-state) level the system reaches after a perturbation. All the other eigenvalues are negative, since $k_{i,j} \geqslant 0$. The time course of the current change is obtained from the sum of the $O(t)$ terms in eqn (5), and can be written

$$I_m(t) = A_0 + A_1 \exp(-r_1 t) + \ldots + A_i \exp(-r_i t), \tag{6}$$

where $i = 2$ for the three-state model and $i = 3$ for the four-state model, $r_i = -\lambda_i$ and $A_0 + A_1 + \ldots + A_i$ are arbitrary constants. Equation (6) is presented in this form to demonstrate its similarity to eqns (7) and (8) below. Since the fractional amplitudes of the exponential components were known from the tail current measurements it was of interest to be able to predict A_i from the model rate constants. Unique A_i values can be calculated from the eigenvectors of the system of differential equations provided the initial conditions are known. The general form of the eigenvectors for the three-state model is

$$u_i = \alpha_i \begin{bmatrix} \dfrac{k_2(\lambda_i + k_4)}{k_3(\lambda_i + k_1)} \\ \dfrac{(\lambda_i + k_4)}{k_3} \\ 1 \end{bmatrix},$$

where α_i is an arbitrary constant evaluated for a given set of initial conditions, and $i = 0 \ldots 2$. Similarly, the general form of the eigenvectors for the four-state model is

$$u_i = \alpha_i \begin{bmatrix} \dfrac{k_2(\lambda_i^2 + (k_4+k_5+k_6)\lambda_i) + k_2k_4k_6}{k_3k_5\lambda_i + k_1k_3k_5} \\ \dfrac{\lambda_i^2 + (k_4+k_5+k_6)\lambda_i + k_4k_6}{k_3k_5} \\ \dfrac{(\lambda_i + k_6)}{k_5} \\ 1 \end{bmatrix},$$

where $i = 0 \ldots 3$. The A_i values for the two models can be obtained by calculating the α_i values for the eigenvectors. This is done by setting $t = 0$ and solving the equation

$$\phi_{33}(0) = (v_0, v_1, \ldots, v_i)\beta = q,$$

where $v_i = u_i/\alpha_i$, β is a column vector with elements α_i and q is a column vector giving the initial fractional occupancy of the channel conformations. The solution, β, is unique since the eigenvectors are linearly independent.

RESULTS

Evidence for a homogeneous population of calcium channels

Calcium currents were isolated by application of sodium and potassium channel blockers and by ion substitution. Sodium currents were eliminated by replacing the external sodium with choline. Potassium currents were suppressed by perfusing internally with CsCl and application of TEA.

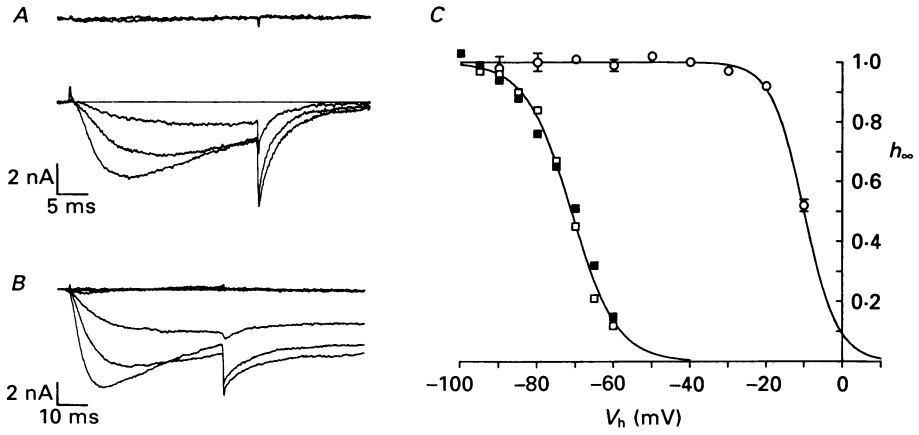

Fig. 1. *A*, the top traces show the current elicited by stepping to −40 and −30 mV from a holding potential of −50 mV. The bottom three traces show the transient calcium current in the same cell activated at −50, −40 and −30 mV, from a holding potential of −80 mV. *B*, the pulse protocol and holding potential were the same as those used in *A*. In this cell there was a significant slow inward tail current following activation of the transient calcium current, which disappeared when the transient calcium current was inactivated. Slow tail currents were also seen after the sustained calcium current and may have been due to activation of a calcium-activated chloride current. *C*, steady-state inactivation (h_∞) of the sustained calcium current was measured by applying a conditioning pulse lasting either 500 or 1000 ms before a test pulse to +20 mV. The normalized magnitude of the inward current during the test pulse (open circles with standard errors, $n = 5$) is plotted against the conditioning potential. The line through the points was drawn by eye. The squares show the inactivation of the transient calcium current in two cells. The normalized peak current recorded at −30 mV is plotted against the initial holding potential. In one case the inactivation was produced by using a 500 ms conditioning pulse; in the other cell the holding potential was adjusted manually.

Since this study was primarily concerned with the kinetics of the sustained calcium current, it was important to ensure that transient calcium currents were not significant. The current illustrated in Fig. 1*A* was identified as the transient calcium current since the time course, activation range (threshold around −50 mV) and steady-state inactivation range appeared to be similar to that recorded previously for this current (Carbone & Lux, 1984). This transient calcium current was not present in every cell and was much smaller than the sustained calcium current, being only a few nanoamperes in amplitude.

The transient calcium current could be selectively removed by using a holding potential of −50 mV, as illustrated by the steady-state inactivation curves for the

sustained (circles) and transient (squares) calcium currents shown in Fig. 1*C*. The curve through the squares in Fig. 1*C* was drawn using eqn (10), with $V_0 = -71$ mV and $K_0 = -6{\cdot}3$ mV. The K_0 value is in reasonable agreement with previous estimates (Bean, 1985; Fedulova *et al.* 1985; Cognard, Lazdunski & Romey, 1986; Fox *et al.* 1987). Cells with a significant inward current at potentials more negative than −20 mV were not used for the analysis of the sustained calcium current.

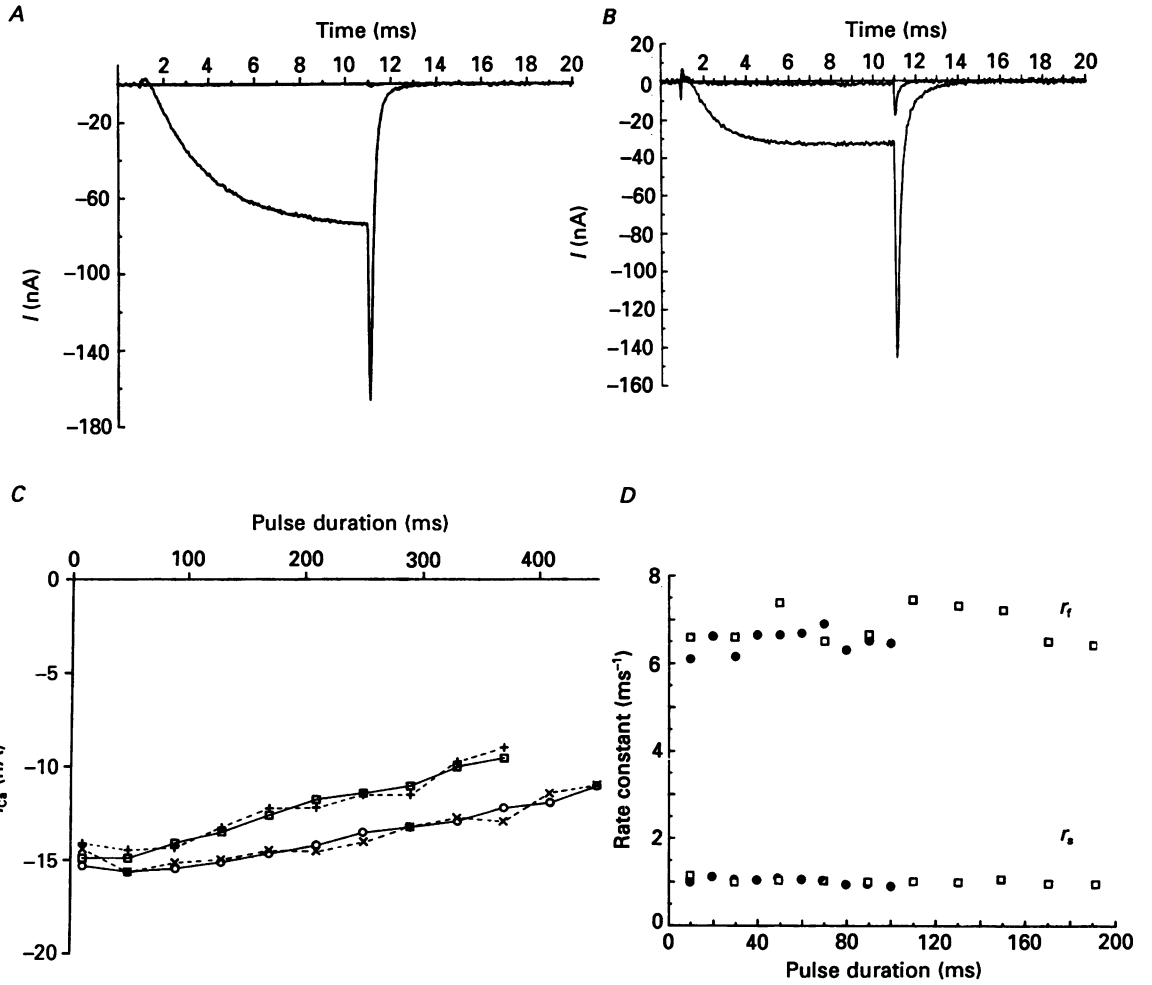

Fig. 2. *A*, both the pulse current and the tail current were completely suppressed when the external calcium was replaced with 10 mM-Co^{2+}. The noise level on the blocked current trace was reduced by signal averaging. *B*, application of 1 mM-Cd^{2+} also suppressed both the pulse and tail currents. A residual tail current was observed upon repolarization due to the voltage dependence of Cd^{2+} block (Byerly *et al.* 1984). *C*, the open symbols show pulse current amplitudes just prior to repolarization. The crosses show the associated tail current amplitudes scaled to overlie the open symbols. The data from two cells are plotted against the activating pulse duration and show that both the pulse- and tail-currents inactivated at the same rate. *D*, the rate constants (eqn (8)) measured from tail currents in two cells (● and □) after pulses of varying duration were independent of the pulse duration.

The N-type calcium channel (Fox *et al.* 1987) did not appear to be present in these cells. In Fig. 1*C*, the h_∞ curve for the sustained calcium current did not increase at negative holding potentials, as expected if the N-type current was absent. The calcium current during long pulses (Fig. 5*B*) did not inactivate significantly, consistent with the absence of N-type channels.

In many cells a slowly decaying inward tail current was observed which persisted long after calcium tail currents had decayed completely (Fig. 1*B*). It was not a component of the calcium tail currents as it was not present in every cell where calcium currents were recorded, but it was blocked by calcium channel blockers, consistent with it being a calcium-activated current. Since sodium and potassium currents were suppressed this current was most probably a calcium-activated chloride current (Miledi & Parker, 1984; Mayer, 1985; Robertson & Taylor, 1986). Cells with a significant slow tail current were not analysed further.

Three observations indicate that the contamination from other currents in the analysed cells was minimal. First, the inorganic calcium channel blockers cobalt (Fig. 2*A*) and cadmium (Fig. 2*B*) suppressed both the inward pulse current and the tail current. Second, during long pulses the tail current inactivated at the same rate as the pulse current. In Fig. 2*C* the crosses show the tail current amplitude scaled to overlie the pulse current amplitude. The close correspondence between the points indicates that there were no contaminating currents activated at +15 mV for pulse durations up to 500 ms. Supporting this conclusion, the two decay rate constants measured from tail currents were independent of the pulse duration (Fig. 2*D*). It is also clear from these data that the calcium current inactivated very slowly under these conditions, and this allowed the activation kinetics to be examined without complications from significant inactivation.

Finally, the pulse and tail currents both disappeared in parallel during the course of the experiment (see Fig. 3*A*). In Fig. 3*B* the filled triangles show the fraction of the peak pulse current, and the open triangles show the fraction of the peak tail current, plotted against the time after commencement of internal perfusion. The close agreement between the two sets of symbols indicated that contamination from other currents was small. The loss of the calcium current from another cell is also shown, illustrating the finding that the calcium current was usually stable for about 10 min after commencement of internal perfusion.

General properties of the sustained calcium current

The results presented indicate that it was possible to record a pure sustained calcium current. The time course of activation and deactivation of this current is illustrated in Fig. 4*A* and *B*. During activation there was a clear delay before the current turned on. The delay became less pronounced as the membrane potential was stepped to progressively more positive potentials and was more obvious in currents recorded at low temperatures (see Fig. 9*A*). Calcium current relaxations after a voltage step were fitted by the sum of two exponential functions. Activation was fitted by the equation

$$I_m(t) = A_0 + A_1 \exp(-r_1 t) - A_2 \exp(-r_2 t), \quad (7)$$

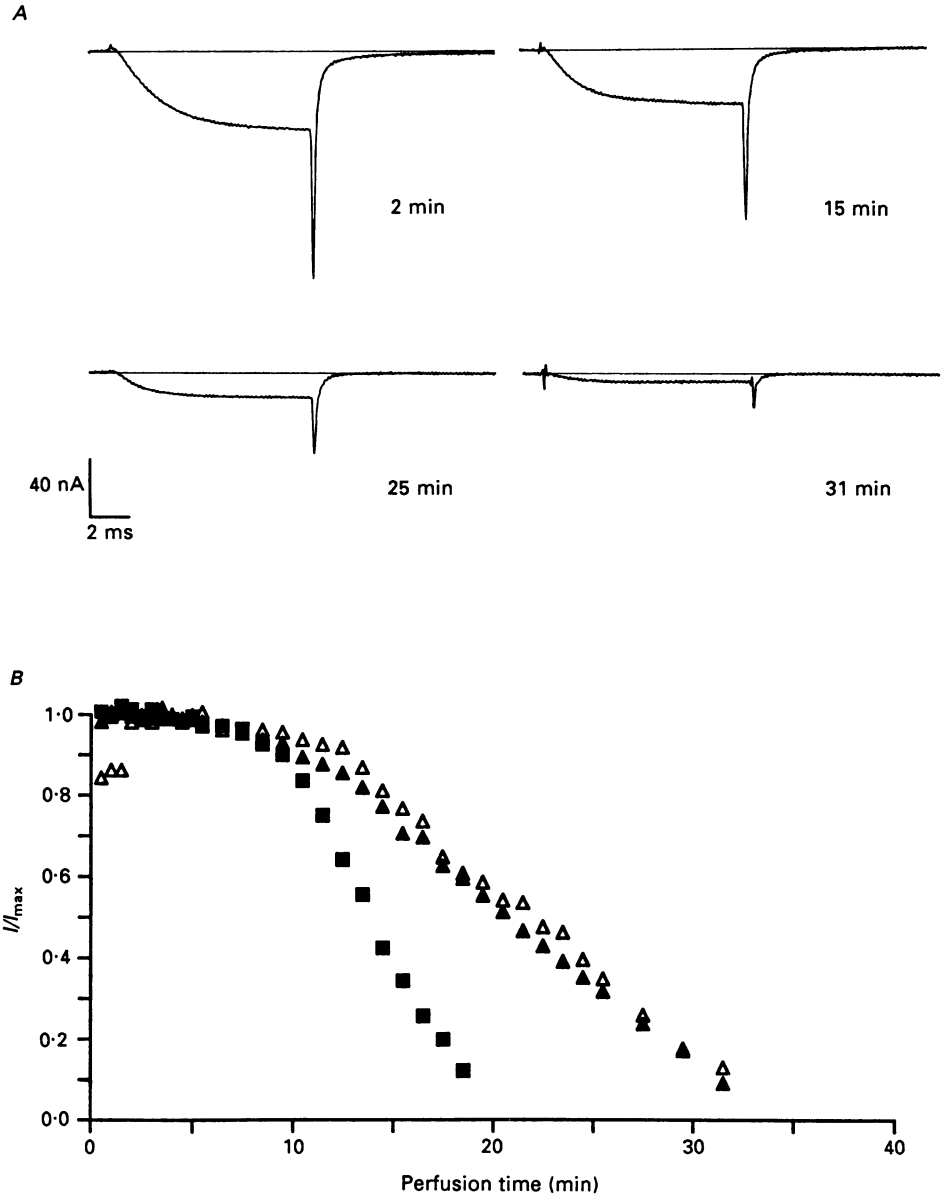

Fig. 3. *A*, calcium currents elicited by test pulses to +15 mV from a holding potential of −50 mV at varying times after the commencement of internal perfusion. *B*, the filled triangles show the pulse current and the open triangles show the peak tail current for the cell illustrated in *A*. The current is plotted as a fraction of the initial value. The pulse and tail currents disappeared in parallel, suggesting that they reflect activation of a pure calcium current. The calcium current disappeared more rapidly in another cell (squares) but initially remained stable for about 10 min.

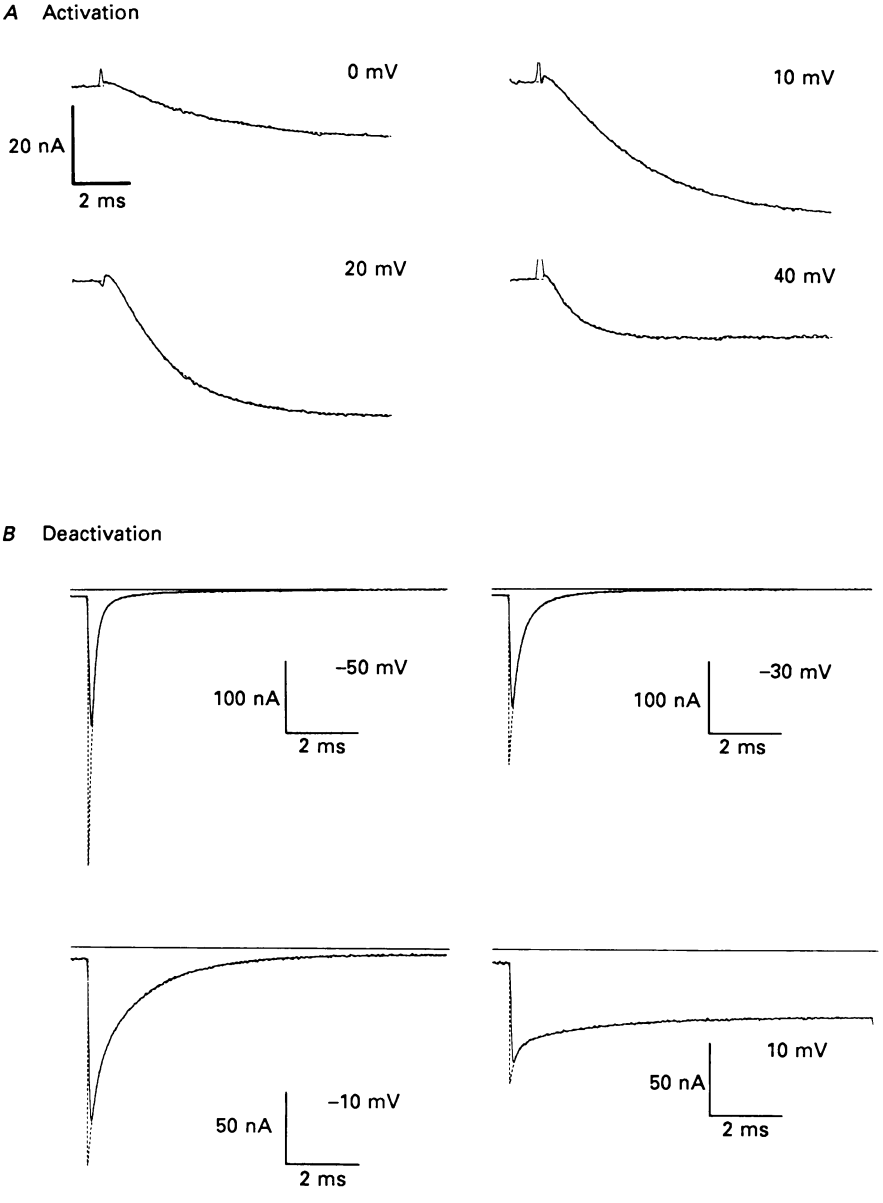

Fig. 4. *A*, activation of the calcium current during pulses to the potentials indicated. A double exponential (eqn (7)) was fitted to the current relaxations using the LMM algorithm. The fitted curves drawn through the data points described the currents accurately. *B*, calcium tail currents recorded at the test potentials indicated, after a 3 ms pulse to +50 mV. The relaxations were again fitted with a double exponential (eqn (8)) using the LMM algorithm. The dotted lines show the best fits to the data, extrapolated back to the time of the voltage step. Note the change in calibration between the top and bottom traces.

where A_0 is a function of the holding potential and gives the final steady-state current level. Similarly, the deactivation (tail) currents were fitted by the equation

$$I_m(t) = A_0 + A_s \exp(-r_s t) + A_f \exp(-r_f t), \quad (8)$$

where A_s is the amplitude of the slower decaying tail current component and A_f is the amplitude of the fast component. Exponential fits to the current relaxations are drawn through the data points in Fig. 4*A* and *B*, and describe the data very accurately (see also Fig. 9*A* and *B*). The equations are presented at this point in order to define the various parameters which will be referred to later in the text. The rate constants will generally be quoted as time constants where $\tau_f = 1/r_f$, $\tau_s = 1/r_s$, $\tau_1 = 1/r_1$ and $\tau_2 = 1/r_2$.

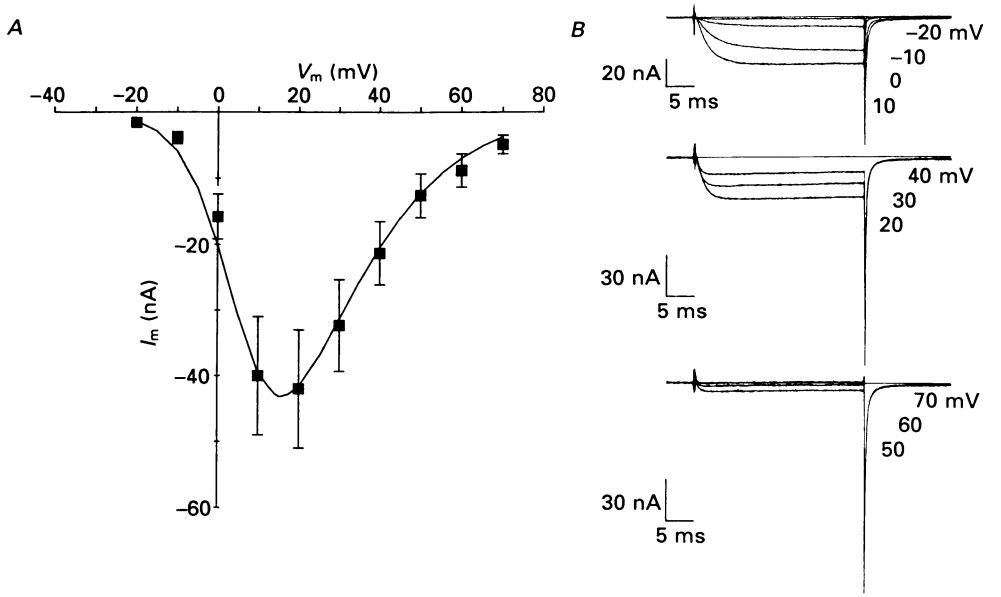

Fig. 5. *A*, the symbols show the average peak inward current recorded in eleven cells. Standard errors are shown where they are larger than the symbols and reflect the variation in the magnitude of the calcium current in the population of cells examined. The line through the points was drawn using eqn (9). The $P_0(V)$ values were taken from the continuous curve in Fig. 6*B* and the $i(V)$ values were taken from the fit to the instantaneous current–voltage relation shown in Fig. 3*B* of the accompanying paper. The curve was scaled to obtain the best fit. The good agreement between the data and eqn (9) indicates that the three sets of data are consistent with the activation of a functionally homogeneous population of channels. *B*, calcium current time course during 30 ms pulses to the test potentials indicated, from a holding potential of −50 mV. These long pulses did not reveal the presence of additional slow exponential activation components. In this cell there was almost no inward or outward current at +70 mV.

The fact that at least two exponentials are required to describe the time course of the whole-cell calcium current is in agreement with the findings of other workers (Fenwick *et al.* 1982; Byerly *et al.* 1984; Dubinsky & Oxford, 1984). The conclusion to be drawn is that a minimal sequential scheme to describe the calcium current must have two closed states preceding an open state.

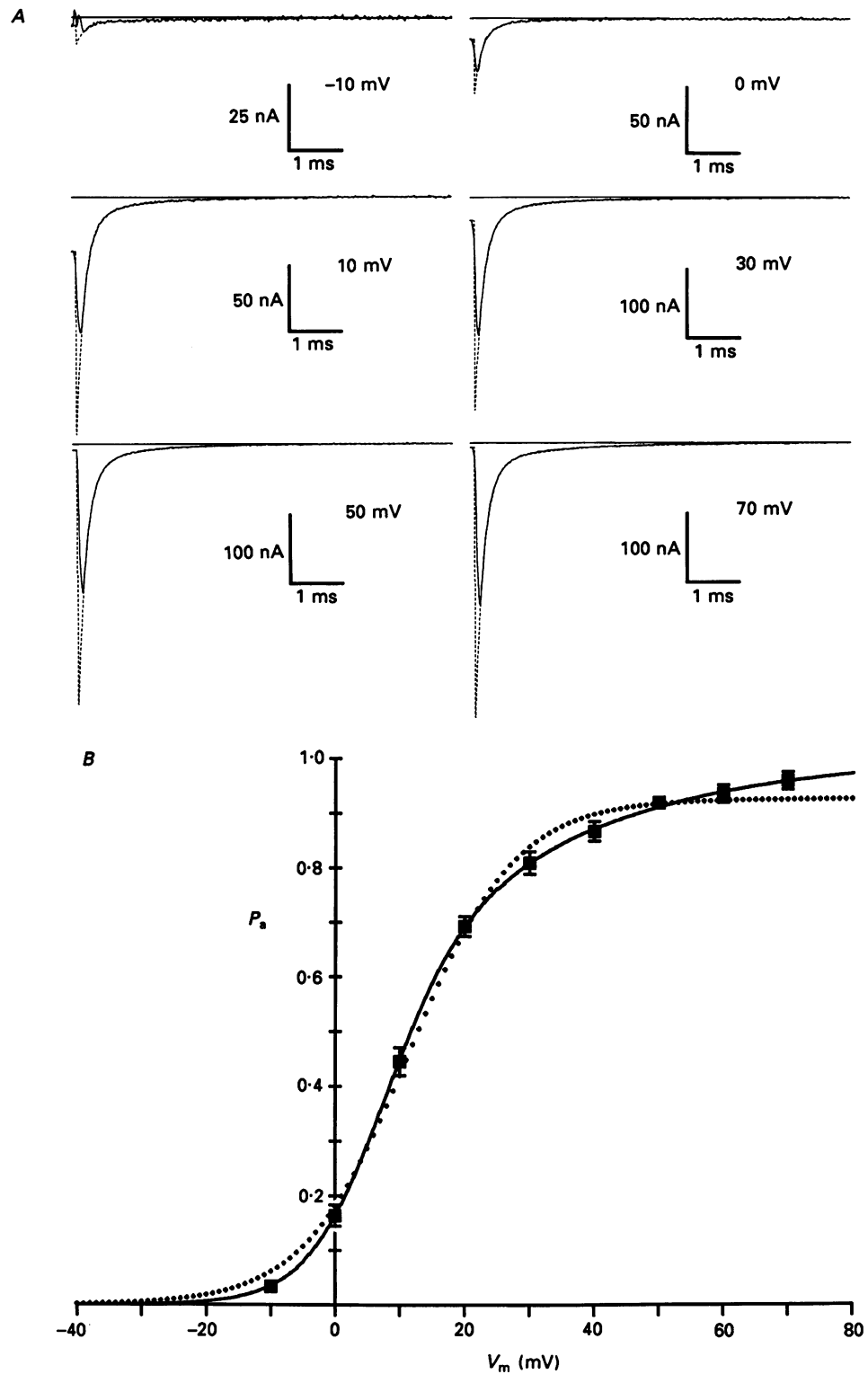

Fig. 6. For legend see facing page.

Steady-state activation

Membrane current due to a specific channel may be described by

$$I_m(V,t) = N\,i(V)\,P_o(V,t), \tag{9}$$

where N is the total number of channels available, $i(V)$ is the single-channel current as a function of membrane potential and $P_o(V,t)$ is the probability that the channel is open as a function of membrane potential and time. Figure 5*A* shows a plot of the steady-state inward current *versus* membrane potential. There is a sharp increase in the inward current at around -10 mV, with a peak at $+10$ to $+20$ mV, after which the inward current declines with further depolarization. The line through the points was obtained using eqn (9) and values for $P_o(V)$ from the smooth curve in Fig. 6*B* and $i(V)$ from the smooth curve in Fig. 3*B* of the subsequent paper.

In the steady state when $t \gg \tau_s$, $P_o(V,t) \rightarrow P_o(V)$, and this function was evaluated by measuring the amplitude of the tail currents at the holding potential of -50 mV after 10 ms activating pulses. Errors introduced by the limited pulse duration were systematic but not significant. Two lines of evidence support this statement. First, the largest activation time constants were recorded at 0 and $+10$ mV and averaged $2{\cdot}72 \pm 0{\cdot}20$ and $2{\cdot}55 \pm 0{\cdot}22$ ms ($n = 11$) respectively, producing errors of less than 3% in the final steady-state current level. Second, the 30 ms activation pulses shown in Fig. 5*B* do not reveal the presence of other slower exponential components during calcium current activation.

Some examples of the tail current measurements are shown in Fig. 6*A* and the normalized, average results from eleven cells are plotted in Fig. 6*B*. The data are characterized by an initial steep rise followed by a slow roll-off. If it is assumed that there is only a single voltage-sensitive reaction during channel activation, then

$$P_o(V) = 1/(1+\exp((V_0 - V_m)/K_0)), \tag{10}$$

where V_0 is related to voltage-insensitive conformational energies and $K_0 = RT/zF$, where z is the magnitude of the equivalent electronic charge which must move across the entire membrane electric field during channel activation. The fit of eqn (10) to the data, using the LMM algorithm, is shown by the interrupted line in Fig. 6*B*. Alternatively, it is possible that there are at least two voltage-sensitive reactions during activation. In this case

$$P_o(V) = 1/(1+E_2+E_2E_1), \tag{11}$$

Fig. 6. *A*, examples of tail current measurements in one cell after activating pulses to the potentials indicated. The interrupted lines show the fitted curve (eqn (8)) extrapolated back to the voltage step time, and the amplitude of this curve was used as an estimate of the peak tail current. *B*, the proportions of the available channels which were active (P_a) were obtained from the tail current measurements. Each point shows the mean $\pm$ the standard error ($n = 11$). The lines show fits of eqn (10) (interrupted line) and eqn (11) (continuous line) to the data. It should be noted that for the models outlined above $P_a(V)$ is equivalent to $P_o(V)$ since the open–closed transition for the calcium channel is voltage sensitive (see Discussion). Therefore these $P_a(V)$ measurements were used as an estimate of $P_o(V)$.

where $E_1 = \exp((V_1 - V_m)/K_1)$ and $E_2 = \exp((V_2 - V_m)/K_2)$ and $K_i = RT/z_i F$. This equation simply predicts the steady-state probability that the channels are open from the three-state model (eqn (3)). The fit of eqn (11) to the data is shown by the continuous line in Fig. 6*B*, and more adequately describes the gradual increase in P_a at positive potentials which was seen in every cell where accurate tail current records were obtained. The parameters were: $V_1 = 13{\cdot}7 \pm 1{\cdot}8$ mV, $V_2 = -9{\cdot}4 \pm 7{\cdot}1$ mV, $K_1 = 7{\cdot}4 \pm 0{\cdot}2$ mV and $K_2 = 25 \pm 5$ mV. K_1 and K_2 correspond to equivalent gating charges of 3·4 e^- and 1·0 e^-, respectively. The result suggests that there are at least two voltage-sensitive reactions during activation of the calcium channel and that the first reaction has a higher voltage sensitivity than the second.

Tail currents

The two rate constants in eqn (8) were measured over an extended potential range by analysis of tail current relaxations. The calcium channels were activated by stepping to +50 mV (at +50 mV, $P_0 \approx 0{\cdot}9$, see Fig. 6*B*) and the tail currents were recorded at return potentials between −70 and +10 mV. Some examples of the measurements are shown in Fig. 4*B*. The average time constants from nine cells are plotted in Fig. 7*A* and *B*. The fast time constant increased steadily from 92 ± 5 μs at −70 mV to 227 ± 20 μs at −20 mV and remained fairly constant between −20 and +10 mV. In contrast, the slow time constant changed gradually from $0{\cdot}62 \pm 0{\cdot}07$ ms at −70 mV to $0{\cdot}92 \pm 0{\cdot}08$ ms at −30 mV and increased sharply between −20 and +10 mV.

The voltage dependence of the underlying reaction rate constants is also reflected in measurements of the fractional amplitude of A_s shown in Fig. 7*C*. At −70 mV A_s represented 9 ± 1% of the total amplitude of the tail current and as the test potential was made more positive the slow exponential contributed a larger fraction to the total relaxation, until a maximum was reached at −10 mV where the amplitude of A_s represented 59 ± 3% of the total.

Activation time course

Two time constants were also measured from the calcium current activation (see Fig. 4*A*), and average values for the time constants from eleven cells are shown in Fig. 7*A* and *B*. Nine of these cells were the same as those used for the tail current measurements; two extra cells were included in which tail current runs were not recorded. At −10 and in some cases 0 mV, and at +50 and +60 mV the currents were too small to adequately resolve more than one exponential component during activation. Activation of the calcium current was dominated by a single exponential (with amplitude A_1 in eqn (7)) which at +10 mV was 8·4 times larger than the second exponential (A_2). The smaller component which accounts for the delay before activation was probably not accurately resolved, and there may have been contributions from asymmetric capacitive currents. For this reason τ_2 and A_2 are not considered in any detail in the analysis that follows. The average values for τ_2 are plotted in Fig. 7*A* for comparison, and show that the fast time constants from the two sets of data were of similar magnitude.

The results presented in Fig. 7 indicate that the relaxation time constants reached

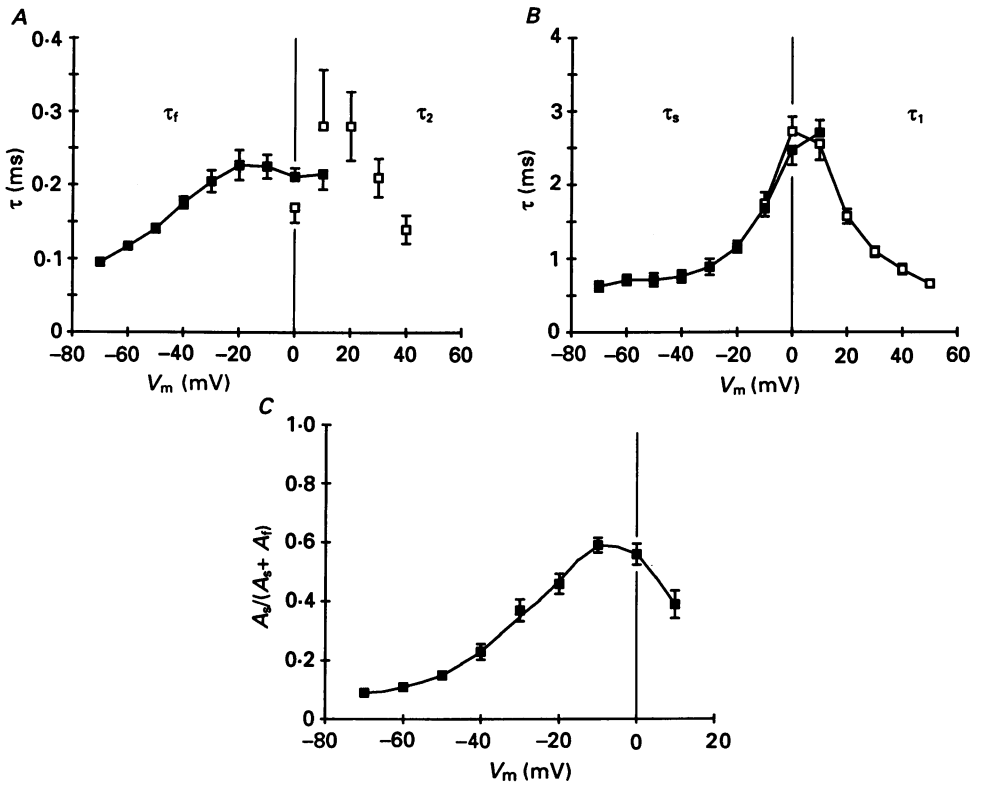

Fig. 7. *A*, fast time constants recorded from activation and deactivation of the calcium current. The filled squares show τ_f recorded from tail currents in nine cells. The error bars are standard errors. The open squares show τ_2 measured from calcium current activation in eleven cells, and the error bars illustrate clearly the uncertainty of these measurements. *B*, slow time constants recorded from activation and deactivation of the calcium current in the same set of cells. The filled squares show τ_s recorded from tail currents and the open squares show τ_1 measured from activation. There is good agreement between the slow time constants at −10, 0 and +10 mV. The lines connect the points. *C*, fractional amplitude of A_s measured from tail currents in nine cells. Standard errors are shown where they are bigger than the symbols. There was a clear peak in this curve at around −10 mV.

a maximum value at around 0 to +10 mV where roughly half the available channels were activated. This type of behaviour is typical of voltage-activated channels and is consistent with sequential schemes where the forward rate constants dominate the kinetics at potentials positive to the half-activation point and the backward rate constants dominate at potentials negative to this point.

Is the three-state model consistent with the data?

The suitability of a three-state scheme for describing the kinetics of the calcium channels was assessed quantitatively by attempting to correlate the steady-state properties with the transient response of the system. The steady-state measurements

provided an estimate of the ratios of the four model rate constants shown in eqn (3). The equations are

$$E_1 = k_2/k_1, \tag{12}$$

$$E_2 = k_4/k_3, \tag{13}$$

where E_1 and E_2 were evaluated from the fit of eqn (11) to the steady-state activation data. The sum, and product of the non-zero eigenvalues of the three-state model, relate the measured rate constants to the model rate constants. The equations are

$$r_1 + r_2 = k_1 + k_2 + k_3 + k_4, \tag{14}$$

$$r_1 r_2 = k_1 k_3 + k_2 k_4 + k_1 k_4. \tag{15}$$

Solving eqns (12)–(15) for k_1 and k_3 gives these two rate constants as solutions to quadratics and therefore there are two sets of k values which satisfy the equations. The two solutions differ in the assignment of the rapid transition. One solution has the $C_2 \leftrightarrow O$ transition being rapid, linked to a slower $C_1 \leftrightarrow C_2$ transition. The other solution reverses these assignments.

The rate constants (r_1, r_2) measured from tail currents were used for the calculations, since both were accurately resolved. If the three-state scheme provides a reasonable description of calcium channel kinetics, then according to eqn (1) the four model rate constants should depend exponentially on the membrane potential. The calculated model rate constants are shown in Fig. 8*A* and *B*. In each case the natural logarithm of the model rate constant is plotted against membrane potential. The lines through the points show that the calculated model rate constants deviate systematically from the expected linear relationship. The results of these calculations suggest that the $P_0(V)$ measurements and the measured voltage dependence of the tail current time constants are not consistent with a three-state model over the voltage range tested.

Assuming that a more complex reaction scheme is applicable, then there may have been other exponential components in the current relaxations which were not resolved. If this were the case then the measured time constants at a given potential may well depend on the initial conditions of the system, due to variability in the magnitude of unresolved exponential components. The initial conditions for a voltage-gated channel are set by the holding potential before the voltage step, therefore one might expect to see a difference in the slow time constant depending on the starting potential. However, τ_s and τ_1 recorded at -10, 0 and $+10$ mV, shown in Fig. 7*B*, are essentially the same suggesting that they represent accurate measurements of a single slow time constant.

Effects of temperature

Experiments were conducted to examine the temperature sensitivity of the time constants. Similar experiments in snail neurones (Brown *et al.* 1983) showed a large discrepancy between the temperature sensitivity of the slow time constant recorded from tail currents and that recorded from activation. It seemed worthwhile to repeat the experiments, to see whether a similar phenomenon was present in these calcium channels.

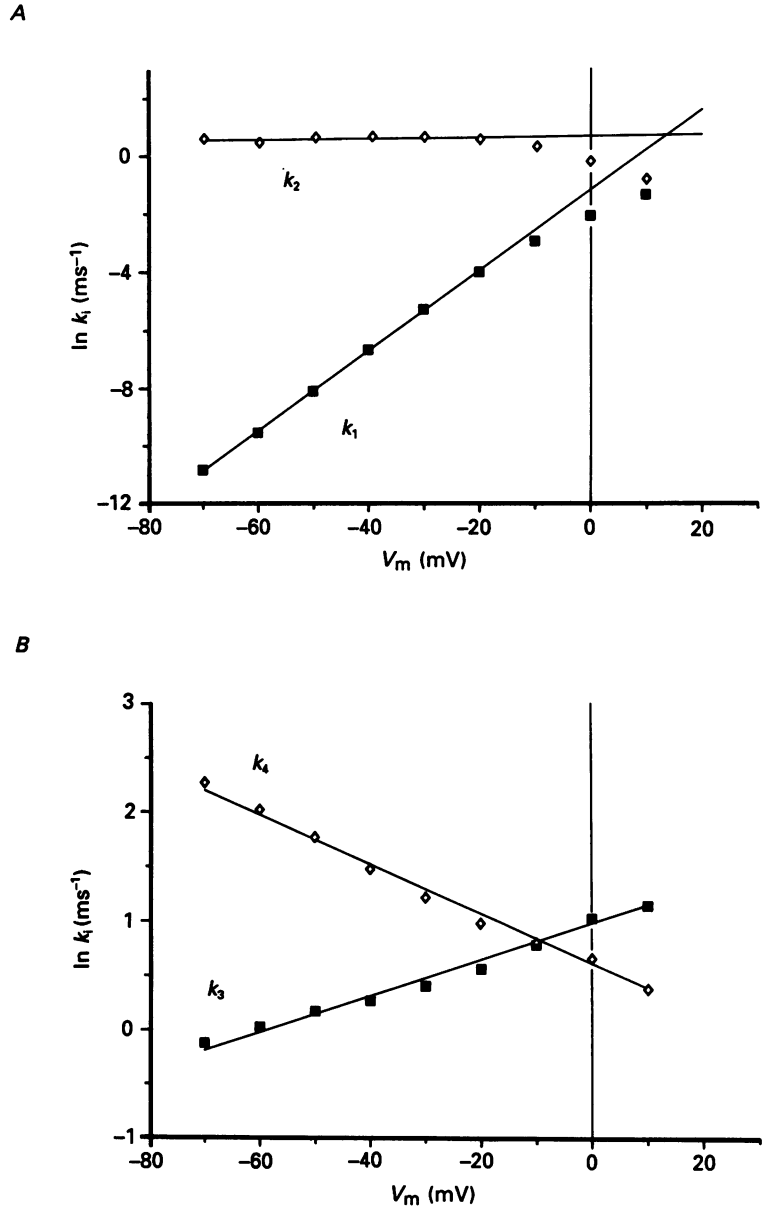

Fig. 8. The three-state model rate constants (eqn (3)) were calculated from eqns (12)–(15) using the tail current data in Figs 6*B* and 7*A* and *B*. The natural logarithm of the calculated rate constants is plotted against membrane potential in *A* and *B*. *A*, the straight lines were drawn through the linear part of the graphs. The calculated values of $\ln(k_1)$ and $\ln(k_2)$ deviated significantly from the expected linear relationship (eqn (1)) at potentials more positive than −20 mV. *B*, the lines through the points illustrate a systematic deviation of the calculated values of $\ln(k_3)$ and $\ln(k_4)$ from the expected linear relationship.

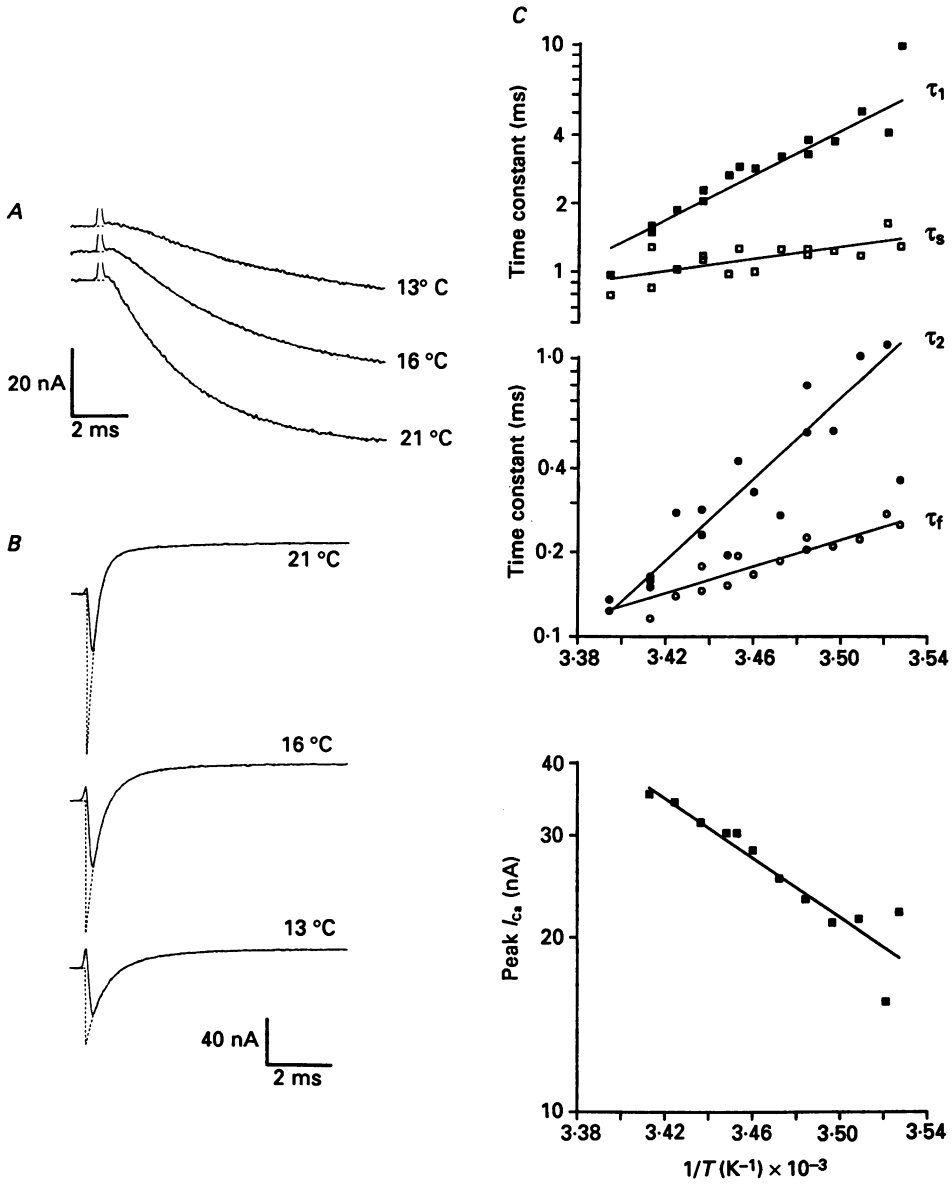

Fig. 9. *A*, sample traces showing the slowing of the calcium channel activation kinetics as the temperature was reduced. Note that the delay before activation of the current is greatly enhanced at 13 °C. *B*, tail currents recorded after the pulses shown above. Note the change in calibration. The interrupted lines through the data in *A* and *B* show that the relaxations were accurately described by a double exponential over the temperature range tested. *C*, the natural logarithm of the parameters is plotted against 1/temperature (K^{-1}). Straight lines were fitted to the data according to the equation $\ln(p) = \ln(p_0) + E_a/RT$, where p_0 is a constant. The apparent activation energy (E_a) obtained from the slope of the lines was used as a measure of the temperature sensitivity of each parameter.

The bath temperature was steadily reduced (1 °C/min), and a test pulse, to +10 mV for 10 ms, was taken each time the temperature dropped by one degree. When the temperature reached 10 °C the process was reversed until the temperature had returned to 20 °C. Slowing of the kinetics was obvious both for the activation

TABLE 1. Temperature sensitivity of parameters measured from calcium currents in three cells. V_h is the holding potential and the apparent E_a (kJ/mol) was calculated as described in the legend for Fig. 9

Parameters	V_h (mV)	$E_a \pm$S.E. (kJ/mol)	Q_{10}
Peak	+10	67±9	2·6
τ_1	+10	85±4	3·4
τ_2	+10	139±15	7·5
τ_s	−50	29±5	1·5
τ_f	−50	79±6	3·1

and deactivation of the calcium current, and results from one cell are presented in Fig. 9*A* and *B*. It was also apparent from these data that reducing the temperature caused a reduction in the peak pulse current. The temperature-dependent reduction in the peak current was not due to the gradual loss of the calcium current, as there was good recovery of the peak current in one cell, where only 15% of the current at 20 °C was lost after 20 min. In the other two cells the data used were obtained within the first 10 min, when the amplitude of the calcium current was generally constant (see Fig. 3*B*).

The effect of temperature was measured as an apparent activation energy (E_a) and some examples of the measurements are shown in Fig. 9*C* with the complete data shown in Table 1. Similar to results for the calcium channels in snail neurones, the slow activation time constant (τ_1) appeared to depend much more strongly on temperature than the slow time constant measured from tail currents (τ_s).

Effects of (±)Bay K 8644

Calcium channels in heart and smooth muscle are sensitive to nanomolar concentrations of these drugs (Brown *et al.* 1984; Hess, Lansman & Tsien, 1984), whereas neuronal calcium channels are unaffected until micromolar concentrations are applied (Nowycky *et al.* 1985). It was of interest to find out what effects, if any, (±)Bay K 8644 had on the kinetic activity of the calcium channels in cat dorsal root ganglion (DRG) neurones.

The effect of 5 μM-Bay K 8644 was only marginal (Fig. 10*A*). Since the effects of 10 μM-Bay K 8644 were larger (Fig. 10*B*), and more consistent, this concentration was used in subsequent experiments. The effects were induced rapidly but were very difficult to wash out. Bay K 8644 increased the steady-state inward current in cells where loss of the calcium current was not large. Figure 10*B* illustrates that at +10 mV the time to peak was shorter and the peak inward current larger after application of 10 μM-Bay K 8644. There was also considerable prolongation of the tail current decay. Bay K 8644 shifted the steady-state activation of the calcium current to more negative potentials, and reduced the slope of the curve. The

normalized average results from five cells are illustrated in Fig. 10*B*. The control data were well described by the previous steady-state activation curve. Fitting the Bay K 8644 steady-state activation data with either eqn (10) or (11) produced lower estimates for the dipole moment of the channel.

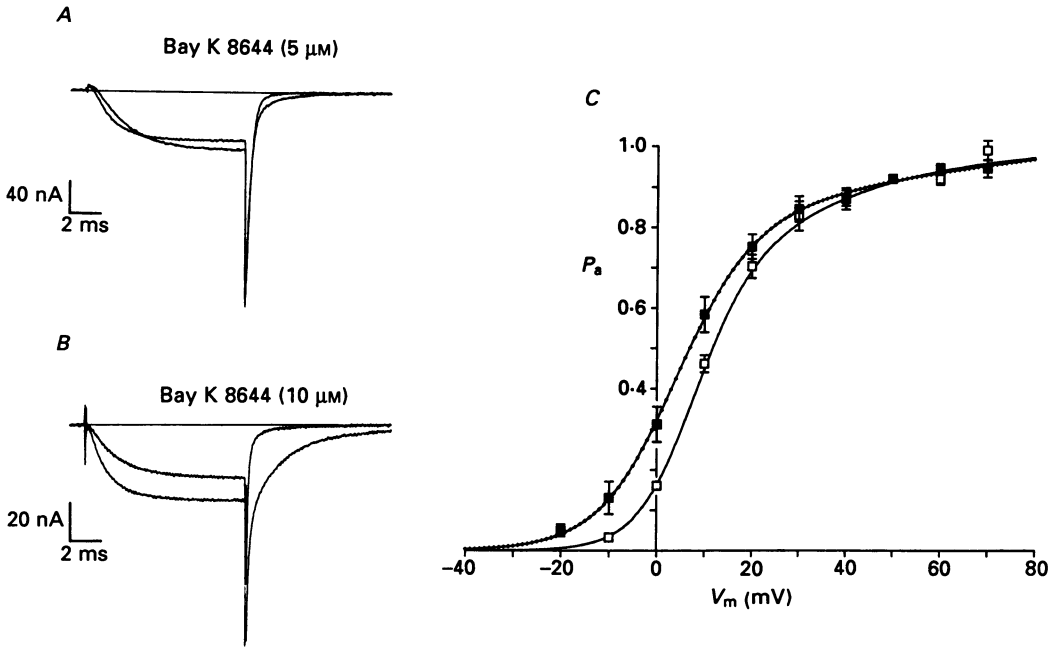

Fig. 10. *A*, the effect of Bay K 8644 during pulses to +10 mV from a holding potential of −50 mV. The control current was larger and slower to activate but faster to deactivate than the current in 5 μM-Bay K 8644. Potentiation of the peak current was not observed presumably due to loss of the calcium current. *B*, in 10 μM-Bay K 8644 there was an increase in the peak inward current at +20 mV, and a significant prolongation of the tail current. *C*, each point shows the normalized average result from five cells, with standard error bars. The open symbols show the control data and the line through the points is the continuous curve replotted from Fig. 6*B*. The filled symbols show the Bay K 8644 data fitted by eqn (11). 10 μM-Bay K 8644 reduced the slope of the steady-state activation curve for the calcium current and shifted the threshold for activation to more negative potentials.

The effects of Bay K 8644 on the relaxation time constants were complex, and are illustrated in Fig. 11. There appeared to be very little change in τ_f after the application of Bay K 8644 (Fig. 11*A*). The magnitude of the effect of Bay K 8644 on the slow time constant was variable from cell to cell. In three out of four cells Bay K 8644 increased τ_s at potentials between −50 and −30 mV, but had little effect at potentials outside this range (Fig. 11*B*). In the one case where Bay K 8644 had little effect on τ_s, it did have an effect on the activation time constant, τ_1. τ_1 was markedly reduced by 10 μM-Bay K 8644 at test potentials between 0 and +50 mV. In all cases Bay K 8644 removed the peak from the τ_1–V plot, and τ_1 decreased monotonically between −20 and +50 mV (Fig. 11*C*).

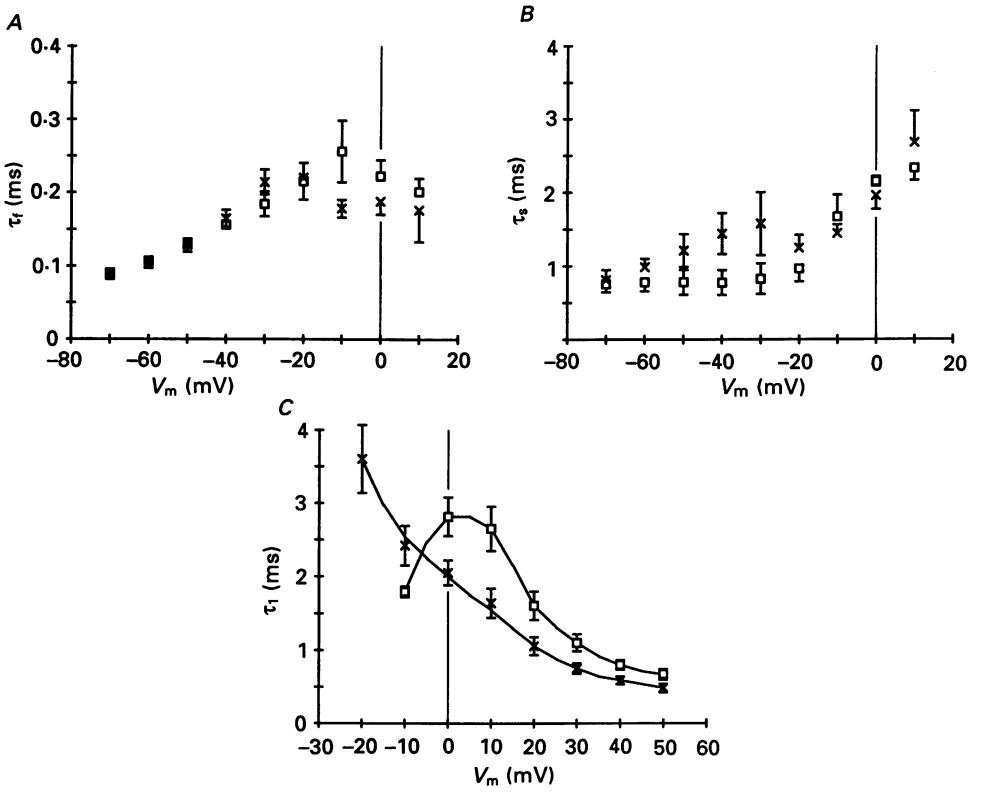

Fig. 11. The squares show the control data and the crosses show the effects of 10 μM-Bay K 8644 on the time constants recorded from calcium currents. Each point shows the average result, with standard errors, from four (*A* and *B*) or five (*C*) cells. *A*, Bay K 8644 did not significantly change τ_f. *B*, on average, τ_s was increased above the control level at potentials more negative than -20 mV. The large standard error bars illustrate the variability of the Bay K 8644 effects. Above -20 mV there was no consistent effect on τ_s. *C*, Bay K 8644 produced a consistent reduction in the predominant activation time constant of the calcium current, and removed the peak from the τ_1–V curve. Lines are drawn through the points by eye.

DISCUSSION

Steady-state measurements

The P_a measurements estimated the fraction of the maximum number of available channels which were conducting in the membrane. The actual probability that a single channel is open (P_o) can only be obtained from single-channel records, but the two estimates will be identical for sequential models if the opening and/or closing reactions are voltage dependent. Thus, previous single-channel studies (Fenwick *et al.* 1982; Lux & Brown, 1984; Reuter, Kokubun & Prod'hom, 1986) and the analysis below suggest that $P_o = P_a$. At present the largest P_o value reported from single-channel analysis is around 0·7 (Reuter, Stevens, Tsien & Yellen, 1982; Reuter *et al.* 1986), although convincing data on the voltage dependence of this parameter showing clear saturation at positive potentials has yet to be obtained.

It was shown that the $P_o(V)$ function was more accurately described by assuming there was more than one voltage-sensitive reaction during activation. A similar-shaped $P_o(V)$ curve was evident in the results of Fenwick *et al.* (1982, Fig. 7*B*), obtained using similar measurement techniques. Kinetic schemes which involve the movement of two or more identical subunits (Hodgkin & Huxley, 1952) will produce a similarly shaped $P_o(V)$ curve.

The steady-state analysis produced estimates for the magnitude of the dipole moments normal to the membrane electric field (Ehrenstein & Lecar, 1977; Stevens, 1978). This is quoted as an equivalent (and therefore not necessarily integral) number of charges moving across the entire membrane electric field. The estimates for the calcium channel of 3·4 e^- for the first and 1·0 e^- for the second reaction are reasonable for a voltage-activated channel. Previous estimates have used eqn (10) to fit steady-state data, giving values of 1·7 e^- in snail neurones (Brown *et al.* 1983) and 1·8 e^- in clonal pancreatic β-cells (Rorsman & Trube, 1986). Calculations using the data shown in Fig. 7*B* of Fenwick *et al.* (1982) suggest that z was approximately 3 e^- for bovine chromaffin cells, consistent with the present study. Uncertainty about the number of voltage-sensitive steps leads to uncertainty about the total dipole moment of the channel protein. Thus, fitting the steady-state data with eqn (10) suggests $z = 3{\cdot}1$ e^-, but for eqn (11) the total dipole moment is 4·4 e^- divided unequally between two steps.

Kinetic measurements

Two time constants were resolved from tail current relaxations in agreement with other studies in cultured and molluscan preparations (Fenwick *et al.* 1982; Brown *et al.* 1983; Dubinsky & Oxford, 1984). The magnitude and voltage dependence of τ_f was very similar to that seen by Fenwick *et al.* (1982) who found that τ_f varied from 0·1 ms at −70 mV to 0·2 ms at 0 mV. In contrast, τ_f in molluscan (0·2 ms; Brown *et al.* 1983, 0·3 ms; Byerly *et al.* 1984) and clonal pituitary tumour cells (0·5 ms; Dubinsky & Oxford, 1984) was constant over a similar voltage range. τ_s was 4–10 times slower than τ_f in agreement with previous data (Fenwick *et al.* 1982; Brown *et al.* 1983; Byerly *et al.* 1984; Dubinsky & Oxford, 1984). In three of these studies, τ_s increased markedly between −70 and 0 mV in good qualitative agreement with the present study.

An attempt was made to relate the steady-state and kinetic measurements using a three-state model. This was done by calculating the four model rate constants from four measured parameters. Although this approach produced reasonable values for the model rate constants at any given potential, the voltage sensitivity of these rate constants was not exponential over the full voltage range tested. However, the values calculated for the model rate constants at 0 mV compare reasonably well with those obtained from single-channel recording techniques (see Table 2).

Consideration of a four-state scheme

One simple modification to the three-state model presented is to include another closed state in the reaction scheme (Fenwick *et al.* 1982). The four-state model was required to account for a number of observations: (1) It should accurately predict the $P_o(V)$ curve shown in Fig. 6*B*. (2) It should reproduce the magnitude and voltage sensitivity of the two time constants measured between −70 and +50 mV and

shown in Fig. 7*A* and *B*. (3) It should also account for the A_s curve between −70 and +10 mV shown in Fig. 7*C*. The calcium channel was assumed to adopt a single open state during activation since single-channel studies indicate that calcium channel open times follow a single-exponential distribution (Fenwick *et al.* 1982; Hagiwara & Ohmori, 1983; Lux & Brown, 1984; Hess *et al.* 1984; Reuter *et al.* 1986). Only two closed states were resolved in these single-channel studies, and the model should be consistent with this observation.

TABLE 2. Comparison of the model rate constants (s^{-1}) at 0 mV calculated for a three-state model with those obtained in previous studies

V_m	k_1	k_2	k_3	k_4	Reference
−5	61	606	345	1230	Fenwick *et al.* (1982)
−30	—	450	1130	530	Cavalie *et al.* (1983)
0	130	350	400	700	Brown *et al.* (1984)
0	130	820	2500	1700	Data above

It seemed reasonable to assume that τ_s and τ_1 represented accurate measurements of a single slow time constant, since the magnitude of τ_s and τ_1 were not dependent on the initial conditions (i.e. the starting potential, see Fig. 7*B*). This slow time constant was used as an estimate of the smallest eigenvalue of the four-state model. A similar assumption was made for the fast time constant although the evidence was not as clear. Even with the uncertainty in the measurement of τ_2, it appeared to have roughly the same magnitude as τ_f at 0 and +10 mV (see Fig. 7*A*), and so $1/\tau_f$ was used as an estimate of the intermediate eigenvalue of the four-state model.

Both the three-state and the four-state models were fitted to the data replotted in Fig. 12, using the direct search algorithm described by Hooke & Jeeves (1960). The data in each graph were simultaneously fitted to the particular model, and all the points were weighted equally during calculation of the sum of the squared deviations. The amplitudes of the exponential components of the tail currents were predicted from the eigenvectors of the model with the initial conditions (fractional occupancy of the various states) calculated for the activation potential of +50 mV. Since estimates were not available for any of the model parameters, all parameters were allowed to vary during fitting. A comparison of the fits of the three-state (interrupted line) and four-state (continuous line) models are shown in Fig. 12. The three-state model was unable to adequately account for the voltage dependence of τ_s or A_s and, consistent with the previous analysis, it was concluded that a three-state model was not suitable. The four-state model was able to account for the data accurately over the voltage range tested and the parameters used were

$$\begin{array}{ccccc} & k_1 = 0{\cdot}27 & & k_3 = 12{\cdot}0 & & k_5 = 2{\cdot}08 & \\ C_1 & \rightleftharpoons & C_2 & \rightleftharpoons & C_3 & \rightleftharpoons & O \\ & k_2 = 12{\cdot}7 & & k_4 = 1{\cdot}25 & & k_6 = 1{\cdot}97 & \\ & \delta_1 = 0{\cdot}49 & & \delta_3 = 0{\cdot}95 & & \delta_5 = 0{\cdot}51 & \\ & z_{12}' = 1{\cdot}91 & & z_{23} = 2{\cdot}59 & & z_{34} = 1{\cdot}15 & \end{array}$$

where $k_{i,j}$ are the 0 mV values in ms^{-1} and z_{ij} are in e^-. The parameters are defined in eqns (1) and (2). Model simulations indicated that the amplitude of the fastest exponential component of the four-state model remained negligible (< 0·01 % of the

total) at test potentials between −70 and +50 mV when stepping from holding potentials of −50 or +50 mV. Thus, this four-state model predicted that the time course of the calcium current should be described by the sum of two exponentials, in agreement with observation. The four-state model follows essentially double-exponential kinetics, since one of the states (C_2) is very short-lived compared to the others.

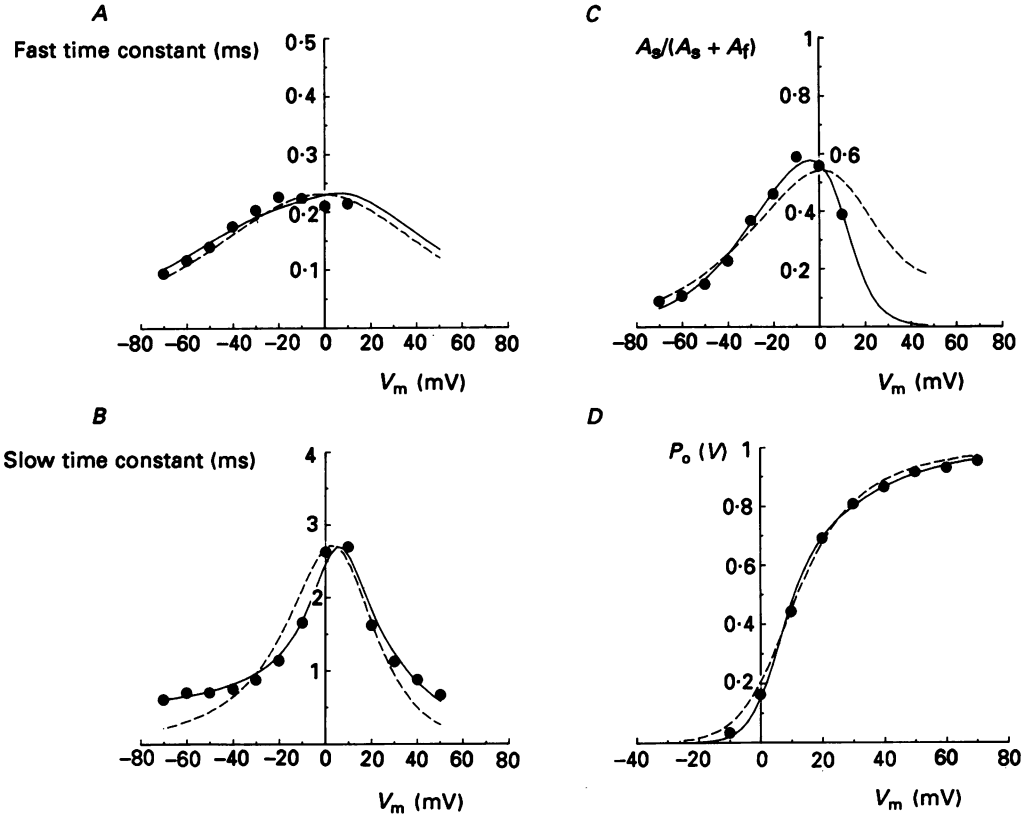

Fig. 12. A comparison of the fits of the three- and four-state models to the data. The data are replotted from Figs 7*A* (*A*), 7*B* (*B*), 7*C* (*C*) and 6*B* (*D*). The values for the slow time constant at −10, 0 and +10 mV in *B* were the average of the two points in Fig. 7*B*. The interrupted lines show the prediction of the three-state model. This model was unable to account for the potential dependence of the slow time constant, and predicted a shallower A_s–V curve which reached a peak at more positive potentials than observed. The predictions from the four-state model are shown by the continuous lines which indicate that this model was able to describe the calcium current accurately over the potential range tested.

Without confidence limits being placed on the parameter estimates, it was not possible to say how well the parameters were defined by the data. However, it was found that the data required the O→C transition to be voltage sensitive (cf. Hagiwara & Ohmori, 1983). If the dipole moment of this reaction step was constrained to be zero ($\delta_5 = 1$) during the fitting routine then τ_f became essentially voltage insensitive, and adequate fits to the data could not be obtained. Thus, the fits

to the data suggest that the mean open time of the channel should be voltage sensitive, consistent with previous single-channel studies (Fenwick *et al.* 1982; Lux & Brown, 1984; Reuter *et al.* 1986). The predicted mean open time ($t_o = 1/k_6$) at 0 mV of 0·5 ms was also in good agreement with these studies.

The four-state model was qualitatively consistent with the double-exponential closed-time distributions measured from single-channel records. The second closed state (C_2) will have a very short mean lifetime of $1/(k_2+k_3) = 40$ μs at 0 mV, and it is unlikely to be resolved due to the bandwidth limitations of single-channel recording. Thus only two closed states will be resolved and a double-exponential closed-time distribution predicted for the single-channel data.

The short-lived conformation, C_2, will have significant effects on the kinetic response of the system; the delay before the first channel opening will be increased by the presence of C_2 since upon reaching this state there is an equal probability ($k_2 \simeq k_3$ at 0 mV) that the channel will return to C_1 or move to C_3. Brown *et al.* (1984) have found that the latency before the first channel opening was longer than that predicted by a three-state model, an observation consistent with the present model.

Temperature effects

The temperature experiments indicated that there was a significant difference in the temperature sensitivity of the slow time constants measured from the turn-on and the tail current measurements. Such a difference might be expected since the membrane potential will change the activation energy at different measurement potentials (Tsien & Noble, 1969). In this case the difference in the apparent E_a values for the slow time constants at -50 and $+10$ mV was 56 kJ/mol. Can the voltage dependence of the channel account for this difference? Assume for simplicity that the channel is opened by a single voltage-sensitive reaction with a dipole moment of 3·1 e^-. This will correspond to an energy difference of 18 kJ/mol between $+10$ and -50 mV, less than half that required to account for the observed difference in the temperature sensitivities. The obvious conclusion is that the two slow time constants reflect different processes. A similar conclusion was reached by Brown *et al.* (1983).

The Q_{10} for the peak current must be corrected for changes in the single-channel current. If it is assumed that the single-channel current has a $Q_{10} \simeq 1{\cdot}2$ (Lux & Brown, 1984), then the Q_{10} of the peak current is reduced to 2·2 (54 kJ/mol). The high Q_{10} observed for the peak current is consistent with previous data (Brown *et al.* 1983; Byerly *et al.* 1984) and suggests that the availability of calcium channels in the membrane is linked to a reaction with a positive enthalpy change.

Effects of Bay K 8644

It is now apparent that (−)Bay K 8644 is the calcium channel agonist while (+)Bay K 8644 has little or no effect (Franckowiak, Bechem, Schramm & Thomas, 1985). Other DHPs also have stereospecific effects (Hof, Peugg, Hof & Vogel, 1985; Perney, Hirning, Leeman & Miller, 1986). Presumably the effects observed here were due to (−)Bay K 8644 binding to some fraction of the calcium channels. Bay K 8644 reduced the slope of the $P_o(V)$ curve, suggesting that it reduced the total dipole

moment of the calcium channel, yet it favoured the open state indicating that it may also change the voltage-independent conformational energies of the channel.

Conclusion

The four-state model outlined provides a quantitative description of the kinetics of the neuronal calcium channel in cat DRG neurones, which is qualitatively consistent with previous single-channel and whole-cell studies. However there are some problems. Both temperature and Bay K 8644 had different effects on τ_s and τ_1, and it is not clear how such results can be reconciled with the model. The model incorrectly predicts that the slow time constant should have a Q_{10} of 2·3 which is relatively insensitive to the membrane potential. This discrepancy is hardly surprising since the temperature data were not of sufficient scope to include in the fitting procedure. A detailed comparison of the effects of both voltage and temperature on calcium channel kinetics is required to address this issue.

This work was completed in partial fulfilment of a Ph.D. degree at the Australian National University under the supervision of Professor P. W. Gage. I am indebted to Professor Gage for his guidance and generous support during the course of this work. I would also like to thank Drs A. J. Gibb and R. Aldrich for helpful comments on the manuscript and Drs R. Fyffe and S. Ghosh for supplying cat ganglia used. W.R.T. was supported by a Department of Education Postgraduate Award.

REFERENCES

ADAMS, D. J. & GAGE, P. W. (1979). Characteristics of sodium and calcium conductance changes produced by membrane depolarization in an *Aplysia* neurone. *Journal of Physiology* **289**, 143–161.

BEAN, B. P. (1985). Two kinds of calcium channels in canine atrial cells. *Journal of General Physiology* **86**, 1–30.

BOSSU, J.-L., FELTZ, A. & THOMANN, J. M. (1985). Depolarization elicits two distinct calcium currents in vertebrate sensory neurones. *Pflügers Archiv* **403**, 360–368.

BROWN, A. M., LUX, H. D. & WILSON, D. L. (1984). Activation and inactivation of single calcium channels in snail neurones. *Journal of General Physiology* **83**, 751–769.

BROWN, A. M., TSUDA, Y. & WILSON, D. L. (1983). A description of activation and conduction in calcium channels based on tail and turn-on current measurements in the snail. *Journal of Physiology* **344**, 549–583.

BYERLY, L., CHASE, P. B. & STIMERS, J. R. (1984). Calcium current activation kinetics in neurones of the snail *Lymnaea stagnalis*. *Journal of Physiology* **348**, 187–207.

CARBONE, E. & LUX, H. D. (1984). A low voltage-activated Ca conductance in embryonic chick sensory neurones. *Biophysical Journal* **46**, 413–418.

CAVALIE, A., OCHI, R., PELZER, D. & TRAUTWEIN, W. (1983). Elementary currents through Ca channels in guinea pig myocytes. *Pflügers Archiv* **398**, 284–297.

COGNARD, C., LAZDUNSKI, M. & ROMEY, G. (1986) Different types of calcium channels in mammalian skeletal muscle cells in culture. *Proceedings of the National Academy of Sciences of the U.S.A.* **83**, 517–521.

CONNOR, J. A. (1979). Calcium current in molluscan neurones: measurement under conditions which maximize its visibility. *Journal of Physiology* **286**, 41–60.

DICHTER, M. A. & FISCHBACH, G. D. (1977). The action potential of chick dorsal root ganglion neurones maintained in cell culture. *Journal of Physiology* **276**, 281–298.

DUBINSKY, J. M. & OXFORD, G. S. (1984). Ionic currents in two strains of rat anterior pituitary tumour cells. *Journal of General Physiology* **83**, 309–339.

EHRENSTEIN, G. & LECAR, H. (1977). Electrically gated ionic channels in lipid bilayers. *Quarterly Review of Physiology* **10**, 1–34.

FEDULOVA, S. A., KOSTYUK, P. G. & VESELOVSKY, N. S. (1985). Two types of calcium currents in the somatic membrane of newborn rat dorsal root ganglion neurones. *Journal of Physiology* **359**, 431–446.

FENWICK, E. M., MARTY, A. & NEHER, E. (1982). Sodium and calcium channels in bovine chromaffin cells. *Journal of Physiology* **331**, 599–635.

FINKEL, A. (1985). Useful circuits for voltage clamping with microelectrodes. In *Voltage and Patch Clamping with Microelectrodes*, ed. SMITH, T. G., LECAR, H., REDMAN, S. J. & GAGE, P. W., pp. 9–24. Bethesda, MD, U.S.A.: American Physiological Society.

FOX, A. P., NOWYCKY, M. C. & TSIEN, R. W. (1987). Kinetic and pharmacological properties distinguishing three types of calcium currents in chick sensory neurones. *Journal of Physiology* **394**, 149–172.

FRANCKOWIAK, B., BECHEM, M., SCHRAMM, M. & THOMAS, G. (1985). The optical isomers of the 1,4-dihydropyridine Bay K 8644 show opposite effects on Ca channels. *European Journal of Pharmacology* **114**, 223–226.

GEDULDIG, D. & GREUNER, R. (1970). Voltage clamp of the *Aplysia* giant neurone: early sodium and calcium currents. *Journal of Physiology* **117**, 217–244.

GLASSTONE, S., LAIDLER, K. J. & EYRING, H. (1949). *The Theory of Rate Processes*. New York: McGraw-Hill Book Company Inc.

HAGIWARA, S. & OHMORI, H. (1982). Studies of calcium channels in rat clonal pituitary cells with patch electrode voltage clamp. *Journal of Physiology* **331**, 231–252.

HAGIWARA, S. & OHMORI, H. (1983). Studies of single-channel currents in rat clonal pituitary cells. *Journal of Physiology* **336**, 649–661.

HAMILL, O. P., MARTY, A., NEHER, E., SAKMANN, B. & SIGWORTH, F. J. (1981). Improved patch-clamp techniques for high-resolution current recording from cells and cell free membrane patches. *Pflügers Archiv* **391**, 85–100.

HESS, P., LANSMAN, J. B. & TSIEN, R. W. (1984). Different modes of Ca channel gating behaviour favoured by dihydropyridine Ca agonists and antagonists. *Nature* **311**, 538–544.

HODGKIN, A. L. & HUXLEY, A. F. (1952). A quantitative description of membrane current and its application to conduction and excitation in nerve. *Journal of Physiology* **117**, 500–544.

HOF, R. P., PUEGG, U. T., HOF, A. & VOGEL, A. (1985). Stereoselectivity at the calcium channel: opposite action of enantiomers of 1,4-dihydropyridine. *Journal of Cardiovascular Pharmacology* **7**, 689–693.

HOOKE, R. & JEEVES, T. A. (1960). 'Direct search' solution of numerical and statistical problems. *American Statistician* **163**, 212–229.

JUNGE, D. & MILLER, J. (1977). Different spike mechanisms in axon and soma of molluscan neurones. *Nature* **252**, 155–156.

KAY, A. R. & WONG, R. K. S. (1987). Calcium current activation kinetics in isolated pyramidal neurones of the CA1 region of the mature guinea-pig hippocampus. *Journal of Physiology* **392**, 603–616.

KOSTYUK, P. G., KRISHTAL, O. A. & DOROSHENKO, P. A. (1974). Calcium currents in snail neurones. I. Identification of calcium currents. *Pflügers Archiv* **348**, 83–93.

KOSTYUK, P. G., VESELOVSKY, N. S. & TSYNDRENKO, A. Y. (1981). Ionic currents in the somatic membrane of rat dorsal root ganglion neurones. II. Calcium currents. *Neuroscience* **6**, 2431–2437.

KRISHTAL, O. A. & PIDOPLICHKO, V. I. (1976). Intracellular perfusion of *Helix* giant neurones. *Neurophysiology* **7**, 258–259.

LEE, K. S., AKAIKE, N. & BROWN, A. M. (1978). Properties of internally perfused, voltage-clamped, isolated nerve cell bodies. *Journal of General Physiology* **71**, 489–507.

LUX, H. D. & BROWN, A. M. (1984). Patch and whole cell calcium currents recorded simultaneously in snail neurones. *Journal of General Physiology* **83**, 727–750.

MAYER, M. L. (1985). A calcium-activated chloride current generates the after-depolarization of rat sensory neurones in culture. *Journal of Physiology* **364**, 217–239.

MEVES, H. & VOGEL, W. (1973). Calcium inward currents in internally perfused giant axons. *Journal of Physiology* **235**, 225–265.

MILEDI, R. & PARKER, I. (1984). Chloride current induced by injection of Ca into *Xenopus* oocytes. *Journal of Physiology* **357**, 173–188.

NOWYCKY, M. C., FOX, A. P. & TSIEN, R. W. (1985). Three types of neuronal Ca channels with different Ca agonist sensitivity. *Nature* **316**, 440.

OSBORNE, M. R. (1976). Non-linear least squares – the Levenberg algorithm revisited. *Journal of the Australian Mathematical Society* B **19**, 343–357.

PERNEY, T. M., HIRNING, L. D., LEEMAN, S. E. & MILLER, R. J. (1986). Multiple calcium channels mediate neurotransmitter release from peripheral neurones. *Proceedings of the National Academy of Sciences of the U.S.A.* **83**, 6656–6659.

REUTER, H., KOKUBUN, S. & PROD'HOM, B. (1986). Properties and modulation of cardiac calcium channels. *Journal of Experimental Biology* **124**, 191–201.

REUTER, H., STEVENS, C. F., TSIEN, R. W. & YELLEN, G. (1982). Properties of single calcium channels in cardiac cell culture. *Nature* **297**, 501–504.

ROBERTSON, B. & TAYLOR, W. R. (1986). Effects of γ-aminobutyric acid and baclofen on calcium and potassium currents in cat dorsal root ganglion neurones. *British Journal of Pharmacology* **89**, 661–672.

RORSMAN, P. & TRUBE, G. (1986). Calcium and delayed potassium currents in mouse pancreatic β-cells under voltage-clamp conditions. *Journal of Physiology* **374**, 531–550.

STANDEN, N. B. (1974). Properties of a Ca channel in snail neurones. *Nature* **250**, 340.

STEVENS, C. F. (1978). Interactions between intrinsic membrane protein and electric field. *Biophysical Journal* **22**, 295–306.

TAYLOR, W. R. (1985). Calcium channel kinetics in mammalian dorsal root ganglion neurones. *Proceedings of the Australian Physiological and Pharmacological Society* **16**, 209*P*.

TSIEN, R. W. & NOBLE, D. (1969). A transition state theory approach to the kinetics of conductance changes in excitable membranes. *Journal of Membrane Biology* **1**, 248–273.